Progress in Organic Coatings 99 (2016) 11–22

Contents lists available at ScienceDirect

Progress in Organic Coatings

journal homepage: www.elsevier.com/locate/porgcoat

Corrosion behaviour of coated steel rebars in carbonated and chloride-contaminated alkali-activated fly ash mortar

M. Criado[a,b,*], I. Sobrados[a], J.M. Bastidas[c], J. Sanz[a]

[a] Materials Science Institute of Madrid (ICMM), CSIC, Sor Juana Inés de la Cruz 3, 28049, Cantoblanco, Madrid, Spain
[b] Department of Materials Science and Engineering, The University of Sheffield, Sir Robert Hadfield Building, Sheffield S1 3JD, UK
[c] National Centre for Metallurgical Research (CENIM), CSIC, Ave. Gregorio del Amo 8, 28040 Madrid, Spain

ARTICLE INFO

Article history:
Received 30 November 2015
Received in revised form 7 April 2016
Accepted 26 April 2016
Available online 21 May 2016

Keywords:
Sol-gel coatings
Alkali activated cement
Corrosion
Carbonation
Chloride
Electrochemical techniques

ABSTRACT

The corrosion behaviour of hybrid organic-inorganic coatings applied on carbon steel embedded in carbonated ordinary Portland cement (OPC) and alkali-activated fly ash (AAFA) mortars and immersed in a 3 wt.% NaCl solution was evaluated using electrochemical methods. The sol-gel coatings were prepared by condensation and polymerization of TEOS/MPTS, TEOS/MTES, TMOS/MPTS and TMOS/MTES mixtures with a molar ratio of 1.0 and deposited by dip-coating on the carbon steel substrates. The coated steels embedded in AAFA mortar presented higher corrosion potential and lower corrosion current density values than those embedded in OPC mortar, indicating that the coatings were more efficient in preventing corrosion of the rebars in this environment. Hybrid coatings synthesized with TEOS/MTES and TMOS/MTES mixtures showed the longest permanence of steel in the passive state when covering rebars embedded in carbonated AAFA mortar. This enhancement of protection may be due to the denser and more compact structure of sol-gel coatings and their greater adhesion to the metallic surface. The study also considered uncoated steel specimens embedded in OPC and AAFA mortars for comparative purposes.

1. Introduction

Concrete is the most widely used construction material in the world with an estimated current consumption of 1 m^3 per person per year [1]. The cement industry is regarded to be responsible for up to 6–7% of all greenhouse gases emitted world-wide, producing 0.85–1.0 t of carbon dioxide (CO_2) per ton of cement. This is mainly a consequence of the calcination of limestone, one of the key ingredients of Portland clinker, which involves the formation and release of CO_2 and high energy consumption during the heating of raw materials in a rotating kiln [1]. Thus the construction industry is very interested in the development of new cementitious binders as an alternative to ordinary Portland cement (OPC).

One of the most promising alternatives is the use of clinker-free cements, known as alkali-activated cements, which are based on wastes and industrial by-products and are produced by the chemical reaction of a poorly crystalline precursor with a highly alkaline solution to form a hardened solid [2]. One of the most widely used precursors for production of alkali-activated cements is fly ash (FA) from the combustion of coal in thermal power stations [3]. Alkali-activated FA (AAFA) has been extensively studied over the past decades [4–7], and its mechanical and durability properties have been seen to be strongly dependent on the type of FA [8] and activating conditions used [9].

Several studies have reported that carbon steel reinforcements are compatible with AAFA mortar [10,11], showing lower corrosion rates than those recorded in OPC mortar. Reinforcing carbon steel embedded in carbonated AAFA mortar specimens partially immersed in a water solution containing 1% (by binder weight) sodium chloride (NaCl) has shown one order of magnitude higher linear polarization resistance (LPR) values than those measured for OPC mortar [10]. The resulting corrosion current density (i_{corr}) was about 0.9 and 0.2–0.5 μA cm^{-2} for OPC and AAFA mortars, respectively, indicating lower corrosion rates in alternative cementitious materials based solely on AAFA. Consistent results have been found in naturally carbonated AAFA concretes, where long-term electrochemical testing showed that the high alkalinity of these systems promoted passivation of the steel rebar during the first 200 days after casting [12]. In the case of alkali-activated concretes based on low-Ca FA, the corrosion potential (E_{corr}) values were within the range of minimal corrosion risk, while higher-Ca FA-based concretes yielded E_{corr} values within the range of high risk of corrosion of the steel rebars.

* Corresponding author at: Materials Science Institute of Madrid (ICMM), CSIC, Sor Juana Inés de la Cruz 3, 28049, Cantoblanco, Madrid, Spain.
E-mail address: m.criado@sheffield.ac.uk (M. Criado).

http://dx.doi.org/10.1016/j.porgcoat.2016.04.040
0300-9440/

Corrosion of reinforcing steel is one of the main causes of the premature failure of reinforced concrete structures (RCS). The passivity of reinforcing steel in concrete is often attributed to the formation on its surface of a thin passive film whose growth and stability is dependent on the high pH of the surrounding concrete [13,14]. The onset of corrosion in RCS can be accelerated by the presence of chloride ions or CO_2. When chloride ions reach the metal/concrete interface they produce pits on the steel surface and localized corrosion takes place [15], while in the presence of CO_2 the passive film may be destroyed when CO_2 reacts with the hydrated cement matrix and lowers the pH (below 9), leading to generalized corrosion attack [16].

Corrosion protection of RCS is often achieved by adding corrosion inhibitors to the concrete, using high performance concrete mixtures, protective coatings, stainless steel rebars, or applying cathodic protection (CP) systems. Of these methods, the use of protective coatings is most attractive because of their low cost compared to other systems such as CP or the use of galvanized steel or stainless steel [17,18].

In recent years the sol-gel process has proven to be a useful method for obtaining protective coatings on a wide variety of materials such as glass [19], ceramics [20], organic materials [21], and metals like copper [22], aluminium and its alloys [23], stainless steel [24] and carbon steel [25]. The sol-gel process is a chemical route based on the hydrolysis of various alkoxides to form the respective silanols [26–28], followed by a condensation reaction between the silanols or the silanols and alkoxides. The sol-gel process involves the evolution of inorganic networks through the formation of a colloidal suspension (sol) and gelation of the sol to form a network in a continuous liquid phase (gel) [29]. The precursors for the synthesis of such colloids are metal or metalloid elements surrounded by various reactive ligands. Metal alkoxides are often used because of their high reactivity with water. The most widely used alkoxides are alkoxysilanes such as tetraethyl orthosilicate (TEOS). There are also other alkoxysilane precursors modified with a polymerizable group, such as epoxy, methacrylic or acrylic organofunctional species, and a common compound with polymerizable organic groups is 3-methacryloxy-propyl-trimethoxysilane (MPTS). The main advantages of this process are the low production cost, high efficiency, good adherence to the substrate, low processing temperature, high homogeneity of the final product and resistance against corrosion and oxidation, homogeneity of the treated surfaces, and high mechanical and chemical resistance.

Depending on their nature, protective sol-gel coatings can be inorganic (when prepared from metal alkoxide precursors) [30] or hybrid organic-inorganic (obtained by including organic groups in the inorganic network to obtain thicker layers and/or flexible films) [31]. Organic-inorganic hybrid materials have attracted particular interest in the microelectronics and optics industries because of their molecular homogeneity, transparency, flexibility, rigidity and durability [27].

In recent studies [32,33] the authors have evaluated the thickness and composition of four types of hybrid organic-inorganic coatings produced with TEOS, MPTS, methyl-triethoxysilane (MTES) and tetramethyl orthosilicate (TMOS) at various molar ratios and analysed their corrosion behaviour when deposited on steel rebars immersed in a simulated concrete pore (SCP) solution contaminated with chloride or in a carbonated synthetic solution simulating the carbonated concrete pore (SCCP) solution. The results show that all the considered organic-inorganic coatings improve the corrosion resistance of carbon steel when exposed to both aggressive media, though their effectiveness is strongly dependent on the nature of the organic reagents used.

In the present study the protective properties of hybrid organic-inorganic coatings prepared via sol-gel with a molar ratio of 1.0 and deposited on carbon steels are assessed using LPR and electrochemical impedance spectroscopy (EIS) methods. The coated rebars were embedded in carbonated OPC and AAFA mortars and immersed in a 3 wt.% NaCl solution for up to 240 days.

Table 1
Chemical composition (% in mass) and Blaine finesses of the tested ordinary Portland cement (OPC) and fly ash (FA).

	OPC	FA
LOI	3.28	6.76
IR	1.04	1.96
SiO_2	21.13	46.32
Al_2O_3	4.16	31.01
Fe_2O_3	3.80	4.50
CaO	63.94	4.90
MnO	0.01	0.05
Na_2O	0.25	0.34
K_2O	0.74	1.34
MgO	0.13	1.29
SO_3	3.06	0.91
Si_{react}	–	36.4
Free CaO	1.28	–
Blaine ($m^2\ kg^{-1}$)	386.7	336

LOI = Loss on Ignition, IR = Insoluble Residue.

2. Experimental methodology

2.1. Preparation of coated steel reinforcing bars

Sol-gel coatings were prepared by condensation and polymerization of TEOS ($Si(OCH_2CH_3)_4$) and MPTS ($CH_2=C(CH_3)COO(CH_2)_3Si(OCH_3)_3$); TEOS and MTES ($(CH_3)Si(OCH_2CH_3)_3$); TMOS ($Si(OCH_3)_4$) and MPTS; or TMOS and MTES. All the organic reagents used were analytical grade from Sigma-Aldrich. As described in detail elsewhere [34], the sol-gel coatings were prepared by mixing 5 g of MPTS or MTES with TEOS or TMOS at a molar ratio of 1.0. This molar ratio was selected on the basis of previous reported results [32–34], where it was determined that a molar ratio of 0.5 was insufficient to obtain a corrosion protective hybrid organic-inorganic film, and that the use of a molar ratio of 2.0 may increase the cost of coating synthesis without improving on the protective properties achieved with coatings produced with a molar ratio of 1.0.

Carbon steel bars of 10 mm in diameter and 100 mm in height were used for the electrochemical tests. Their chemical composition (% by weight) was: 0.45C, 0.22 Si, 0.72 Mn, <0.010 P, 0.022 S, 0.13Cr, 0.13 Ni, 0.18Cu, and balance Fe. The carbon steel bars were dipped in the hybrid organic-inorganic solutions, withdrawn at a rate of 14 mm min^{-1}, and air-dried for approximately 10 min. This procedure was carried out twice, after which the coated steels were heated at 65 °C for 24 h and cured at 160 °C for 3 h.

2.2. Preparation of prismatic mortar specimens

A type I (42.5 R) commercial Portland cement and a Class F FA obtained from a steam power plant in Córdoba (Spain) were used as binding materials to produce the mortar slabs. The chemical composition and Blaine fineness of the materials (Spanish/European Standard UNE-EN 196-6) are shown in Table 1.

As alkaline activator a solution containing 85 wt.% 10 M NaOH and 15 wt.% sodium silicate was used. The reagents used to prepare this solution were laboratory grade sodium hydroxide (NaOH) pellets (Panreac) and sodium silicate or waterglass containing 27% SiO_2, 8.2% NaOH and 64.8% H_2O (Merk). The sand:OPC and sand:FA ratio used in the mortars was 3.0. A standardized, evenly graded siliceous sand was employed (99% SiO_2 content, with 65% particle size <1 mm and 35% <0.5 mm). In all mortar types the liquid:binder ratio was 0.6 in order to favour the carbonation process.

Table 2
Hardening (Step I and Step II), carbonation (Step III) and exposure steps for reinforced mortar specimens. During Step IV carbon steel reinforced specimens were partially immersed in a 3 wt.% NaCl solution.

Step	OPC Mortar	AAFA Mortar
I	24 h at room temperature, 100% RH	24 h in oven at 85 °C, 100% RH
II	28 days in a humidity chamber (98% RH, 20 ± 2 °C)	
III	60 days in a carbonation chamber at a 43.2% RH in a K_2CO_3 solution. The chamber was CO_2 saturated by filling it with the gas two times a day [32]	
IV	240 days of partial immersion in a 3 wt.% NaCl solution	

Prismatic mortar specimens similar to those used in a previous work [35] were prepared with dimensions of 8 cm × 5.5 cm × 2 cm and two embedded carbon steel bars, as illustrated in Fig. 1. Two specimens were made for each mortar/steel system, giving four test bars for each condition. The OPC and AAFA mortars were subjected to hardening and carbonation steps in the conditions specified in Table 2 [36] and subsequently, without any prior water pre-saturation, the specimens were partially immersed (2.5 cm from specimen bottom) in a 3 wt.% NaCl solution for up to 240 days at room temperature and open to the air.

Completion of the carbonation reaction was checked with cubic samples (side 10 cm) produced and carbonated under similar conditions to those specified for the reinforced slabs (Table 2). The cubes were sectioned at different CO_2 exposure times and the carbonation depths were monitored by spraying the freshly cut surfaces with a 1% phenolphthalein solution.

Fig. 1. Photograph of one of the studied prismatic mortar specimens.

2.3. Electrochemical measurements

E_{corr}, LPR and EIS measurements were recorded after 1, 7, 30, 60, 90, 120 and 240 days of partial immersion of the specimens in a 3 wt.% NaCl solution. The NaCl solution was replaced with a fresh solution after each measurement in order to avoid contamination of the electrolyte and to maintain constant the chloride concentration in the solution.

For the electrochemical measurements a conventional three-electrode configuration cell was used, consisting of an external stainless steel cylinder of 5 cm in diameter with a centrally drilled hole as counter electrode, a saturated calomel electrode (SCE) placed in the hole as reference electrode, and the coated or uncoated steels embedded in the prismatic mortars as working electrode. A pad soaked in tap water was used to facilitate the electrical measurements. The exposed steel surface area on the working electrode was controlled by covering it with adhesive tape and leaving an active surface area of 10 cm^2.

A PARC 273A Potentiostat and a Solartron 1250 FRA were utilized for the electrochemical measurements. LPR was obtained by applying a ΔE of ±15 mV vs. E_{corr}, at a scan rate of 0.1667 mV s^{-1}. The i_{corr} was calculated using the Stern-Geary equation [37]: $i_{corr} = B/R_p$, adopting a tentative B value of 52 mV or 26 mV for carbon steel in the passive or active (corroding) state, respectively [38]. EIS measurements were recorded at the E_{corr} in a frequency range from 64 kHz to 10 mHz with a logarithmic sweeping frequency of 5 points per decade. EIS involved the imposition of a 10 mV rms amplitude excitation voltage. Both LPR and EIS measurements were performed after the E_{corr} was stabilized for at least 30 min.

3. Results and discussion

3.1. Evolution of corrosion potential and corrosion current density

Fig. 2 shows the variation in E_{corr} for carbonated OPC mortar specimens with uncoated and coated steel rebars as function of the immersion time in 3 wt.% NaCl solution. The E_{corr} of the uncoated rebar embedded in OPC mortar always shows very negative values (between −570 and −640 mV vs. SCE) throughout the exposure time. According to ASTM C876-09 standard [39], if the E_{corr} of a reinforcement embedded in concrete is more negative than −270 mV vs. SCE, there is a high risk of corrosion with 90% probability. The E_{corr} of the coated rebars embedded in OPC mortar, as shown in Fig. 2, is between −560 and −690 mV vs. SCE, corresponding to an active state. These shifts in the E_{corr} to more negative values also indicate that the mortar present low resistivity. Typical E_{corr} ranges of carbon steel in low resistivity concrete (wet and chloride-contaminated) are between −400 and −600 mV vs. SCE, according to RILEM TC 154-EMC Recommendations [40]. Similar values are obtained for the uncoated steel in the first days of immersion. The initiation of corrosion on the uncoated steel rebar embedded in the mortar specimen is probably a consequence of the breakdown of the passive film induced by the chloride ions, given that the specimens present low resistivity (more open pore structure) which allows the transport of chlorides into concrete [41,42]. For

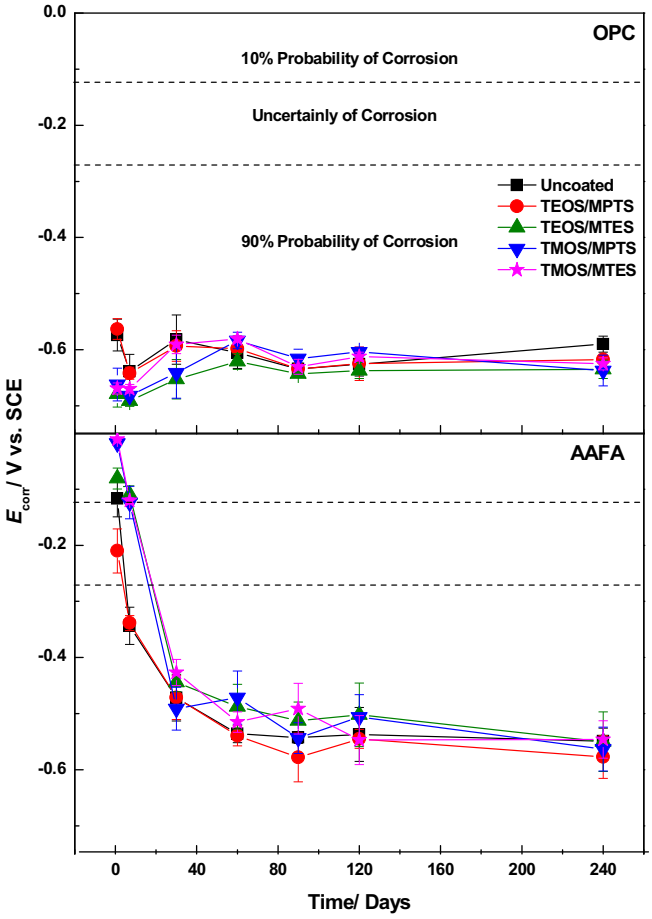

Fig. 2. Corrosion potential (E_{corr}) evolution of uncoated and coated steel rebars embedded in carbonated OPC and AAFA mortars over immersion time in a 3 wt.% NaCl solution.

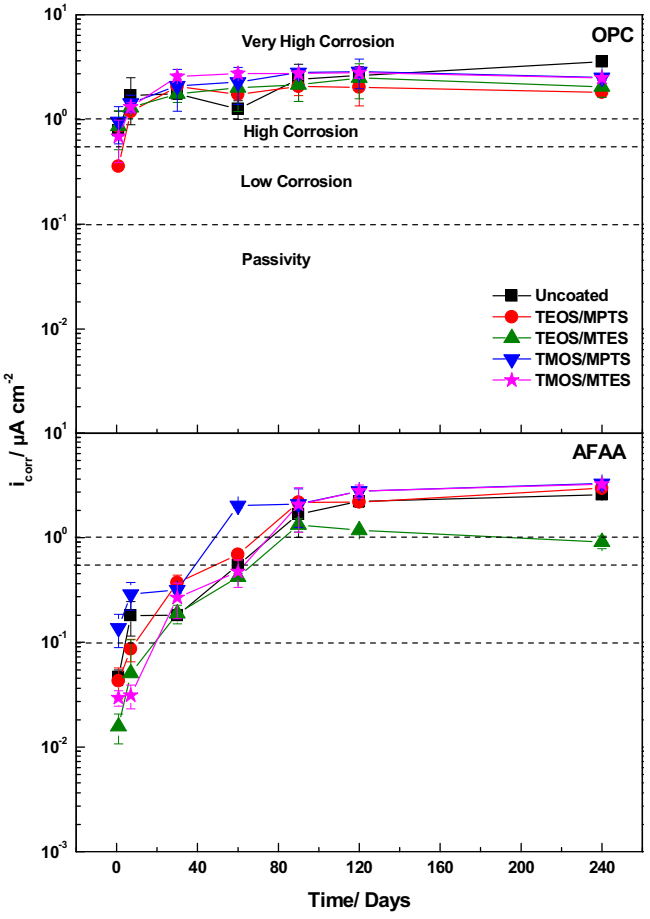

Fig. 3. Corrosion current density (i_{corr}) evolution of uncoated and coated steel rebars embedded in carbonated OPC and AAFA mortars over immersion time in a 3 wt.% NaCl solution.

specimens with a coated steel rebar, the corrosion mechanism is probably controlled by chloride penetration through defects in the coating initiating the corrosion process.

For the carbonated AAFA mortar immersed in the NaCl solution it is seen (Fig. 2) that both the uncoated steel rebars and those coated with polysiloxane hybrids synthesized from the TEOS/MPTS mixture cross the threshold potential limit of −270 mV vs. SCE within 7 days of exposure, indicating a more than 90% possibility of the occurrence of corrosion. The E_{corr} of the other coated steel rebars is −270 mV vs. SCE up to 30 days of immersion, and then shifts negatively to about −550 to −580 mV vs. SCE. These coated rebars remain in a passive state for a longer time (between 7 and 30 days instead of 1 and 7 days).

The i_{corr} values measured using the LPR method for the uncoated and coated steel rebars embedded in carbonated systems at different exposure time intervals are shown in Fig. 3. The criteria used to analyse these results are based on the state of corrosion of steel in concrete reported in [43–45], where a i_{corr} of <0.1 µA cm^{-2} corresponds to passivity, 0.1 µA cm^{-2} < i_{corr} <0.5 µA cm^{-2} corresponds to low corrosion, 0.5 µA cm^{-2} < i_{corr} <1.0 µA cm^{-2} to high corrosion, and i_{corr} > 1.0 µA cm^{-2} to very high corrosion. The i_{corr} of the uncoated rebar embedded in OPC mortar specimens is 0.8 µA cm^{-2} after 7 days of immersion, a high corrosion level, and increases rapidly to 1–10 µA cm^{-2} for longer chloride exposure times, indicating very high corrosion. The coated steel rebar with polysiloxane hybrids synthesized from the TEOS/MPTS mixture has the lowest i_{corr} at 7 days of exposure (see Fig. 3). However, a progressive increase in the i_{corr} value is observed for coated rebars with the other organic-inorganic films due to their deterioration in the presence of chloride ions, indicating that their protective properties are not always good.

The i_{corr} values of uncoated and coated rebars embedded in carbonated AAFA mortar specimens immersed in 3 wt.% NaCl solution are also shown in Fig. 3. During the first days of immersion (~1 week) all the steel rebars exhibit i_{corr} values of the order of 0.05 µA cm^{-2}, except for the uncoated steel and the coated steel rebars with organic-inorganic hybrids synthesized from the TMOS/MPTS mixture, whose i_{corr} values are higher (0.18 µA cm^{-2} and 0.29 µA cm^{-2}, respectively). After 60 days of immersion the corrosion level for the uncoated steel and the coated steel rebars with organic-inorganic hybrids synthesized from the TMOS/MPTS and TEOS/MPTS mixtures is high (0.5 µA cm^{-2} < i_{corr} < 1 µA cm^{-2}), while that of the other coated rebars is low (0.1 µA cm^{-2} < i_{corr} < 1 µA cm^{-2}) [43–45]. After 90 days of immersion all the specimens present similar i_{corr} values of around 1.9 µA cm^{-2}. These values remain roughly constant throughout the immersion time, except for the coated steel rebar with organic-inorganic hybrids synthesized from the TEOS/MTES mixture, which exhibits the lowest i_{corr} value. This coated steel rebar embedded in carbonated AAFA mortar exhibits the best protective properties over the 240 days of immersion.

The higher E_{corr} values and the lower i_{corr} values of the TEOS/MTES and TMOS/MTES coated steel rebars embedded in carbonated AAFA mortar may be attributed to the establishment of a physical barrier to aggressive ions by the deposition of these more protective coatings on the metal surface.

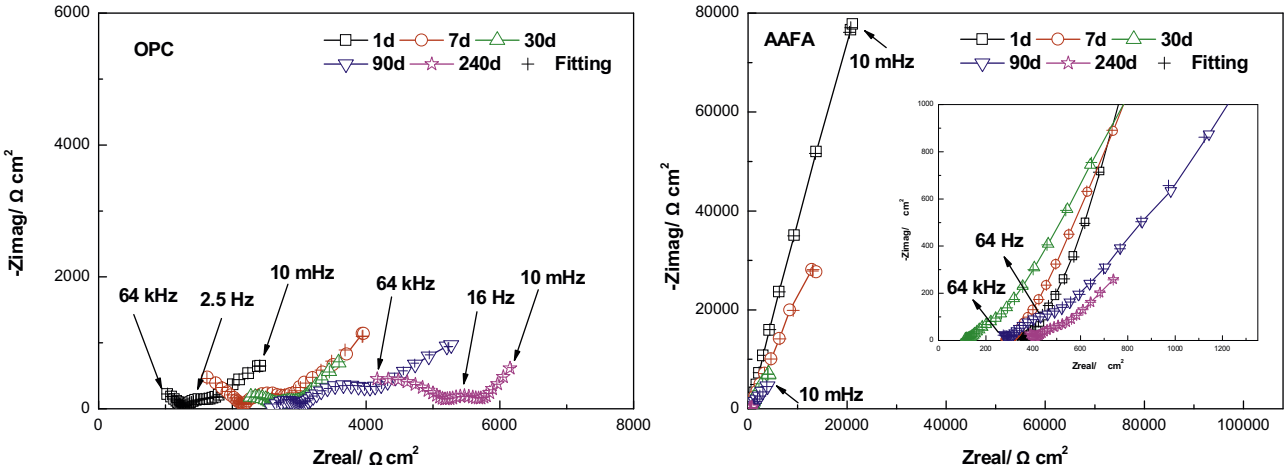

Fig. 4. Nyquist plots for uncoated steel rebars embedded in carbonated OPC and AAFA mortars over 240 days of immersion in a 3 wt.% NaCl solution.

In the light of the results, the type of cementitious matrix (OPC or FA) had a notable influence on the onset of corrosion on the coated steel rebars. This is to be expected, as the two systems present wide differences in terms of the chemical composition of their main reaction products: calcium silicate hydrate (C–S–H) gel in the hydration of Portland cement [46] and the alkali aluminosilicate hydrate (N–A–S–H) gel generated as a result of FA activation [47]. Therefore, the reaction mechanisms involved in the production of the two types of gel and in the kinetics of the formation processes influence on the onset of corrosion. It is also important to stress that the exact chemical composition of the pore solution of the cementitious matrix is quite complex to determine, and varies with the type of cement, water:cement ratio, degree of hydration and exposure conditions, and therefore the presence of certain species in the pore solution could influence the corrosion process.

Porosity is known to affect not only mechanical strength but durability as well, as high porosity allows aggressive agents like chloride ions to penetrate the material. Fernández-Jimenez et al. [48] determined the effective porosity and pore size distribution in OPC and AAFA mortars. The specimens used were similar to those tested in the present research but with a different liquid:binder ratio. OPC and AAFA with a sodium silicate and sodium hydroxide solution presented porosity values of 7.6 and 9.6%, respectively. These values were very similar and suggest that the two materials could present comparable corrosion performance. Another study carried out by the authors [11] also indicates the presence of comparable permeability in OPC and AAFA mortars, using the same liquid:binder ratio employed in this study. The results show that at the end of the exposure time the carbonated mortars presented a pH value of about 9.5 and the soluble chloride concentration (in wt.% vs. binder) was: 0.44 ± 0.11 in OPC and 0.37 ± 0.06 in AAFA with sodium silicate and sodium hydroxide solution.

It should also be noted that the FA was activated with a blend of NaOH and sodium silicate, and therefore the electrolyte present in these mortar pores may act as a corrosion inhibitor to hinder steel corrosion. Silicate anions are known to be corrosion inhibitors for iron and steel [49,50]. These authors observed that Fe(II) dissolution current values were smaller in the solution containing silicate, which may be explained by assuming that the ionic resistivity of the passive film is greater when silicate is present in the solution. This behaviour is probably due to its incorporation in the film, which reduces the dissolution of ferrous species. Therefore, the significant silicate concentration in the electrolyte of AAFA mortar may be the cause of the better corrosion behaviour of steel in this mortar than in OPC mortar.

On the other hand, the TEOS or TMOS/MTES formulations had a denser and more compact structure, with a degree of condensation of between 82–85% and a *d* parameter between 2.86–2.99 [34]. Moreover, these coatings presented a large number of covalent bonds, a higher atomic percentage of Si in their compositions [33], and strong adhesion between the coating and the steel substrate, and thus less susceptibility to debonding and delamination of the coatings. Therefore these polysiloxane hybrid films provided a more effective physical barrier which prevented the penetration of the electrolyte, promoting a lower corrosion susceptibility in carbonated AAFA mortar for up to 60 days of exposure in a chloride-rich solution.

3.2. EIS results

Fig. 4 shows Nyquist plots for uncoated steel rebars in carbonated OPC and AAFA mortars over 240 days of immersion in 3 wt.% NaCl solution. The plots show three time constants regardless of the immersion time. At frequencies above 10^3 Hz the spectra show a semicircle characterising the dielectric properties of the bulk matrix [51]. In some cases, only a section of this semicircle is observed within the available instrument frequency range. The second time constant in the intermediate frequency range (usually in the 10^3–1 Hz range for OPC mortar and in the 10^3–10 Hz range for AAFA mortar) is attributed to the properties of the passive layer formed on the steel rebar due to the high pH of OPC or AAFA pore solutions. The third time constant in the low frequency range (<1 or 10 Hz for OPC or AAFA mortars, respectively) is related to the interface properties between the steel rebar and mortar where corrosion took place, namely charge transfer resistance (R_{ct}) and double-layer capacitance (Y_{dl}).

Fig. 5 depicts Nyquist plots for coated rebars embedded in carbonated OPC and AAFA mortars over 240 days of immersion in 3 wt.% NaCl solution. These specimens also present three time constants, which appear in the same range of frequencies as those observed for the uncoated rebars in both mortars (Fig. 4), except for the first time constant of OPC mortar which appears at frequencies above 10^2 Hz. In the case of the coated rebars, the first time constant is also attributed to the dielectric properties of the bulk matrix, the second is associated with the presence of the hybrid coating layer, and the third is also related to the corrosion process occurring at the steel/mortar interface. In the AAFA system the three time constants are more difficult to see, since the capacitance values are very close (between 10^{-5} and 10^{-4} F cm^{-2} $s^{-(1-\alpha)}$) and even overlapping. In contrast, in the case of the OPC system the capacitance values at high frequencies appear between $10^{-8} - 10^{-7}$ F cm^{-2} $s^{-(1-\alpha_{HF})}$, at

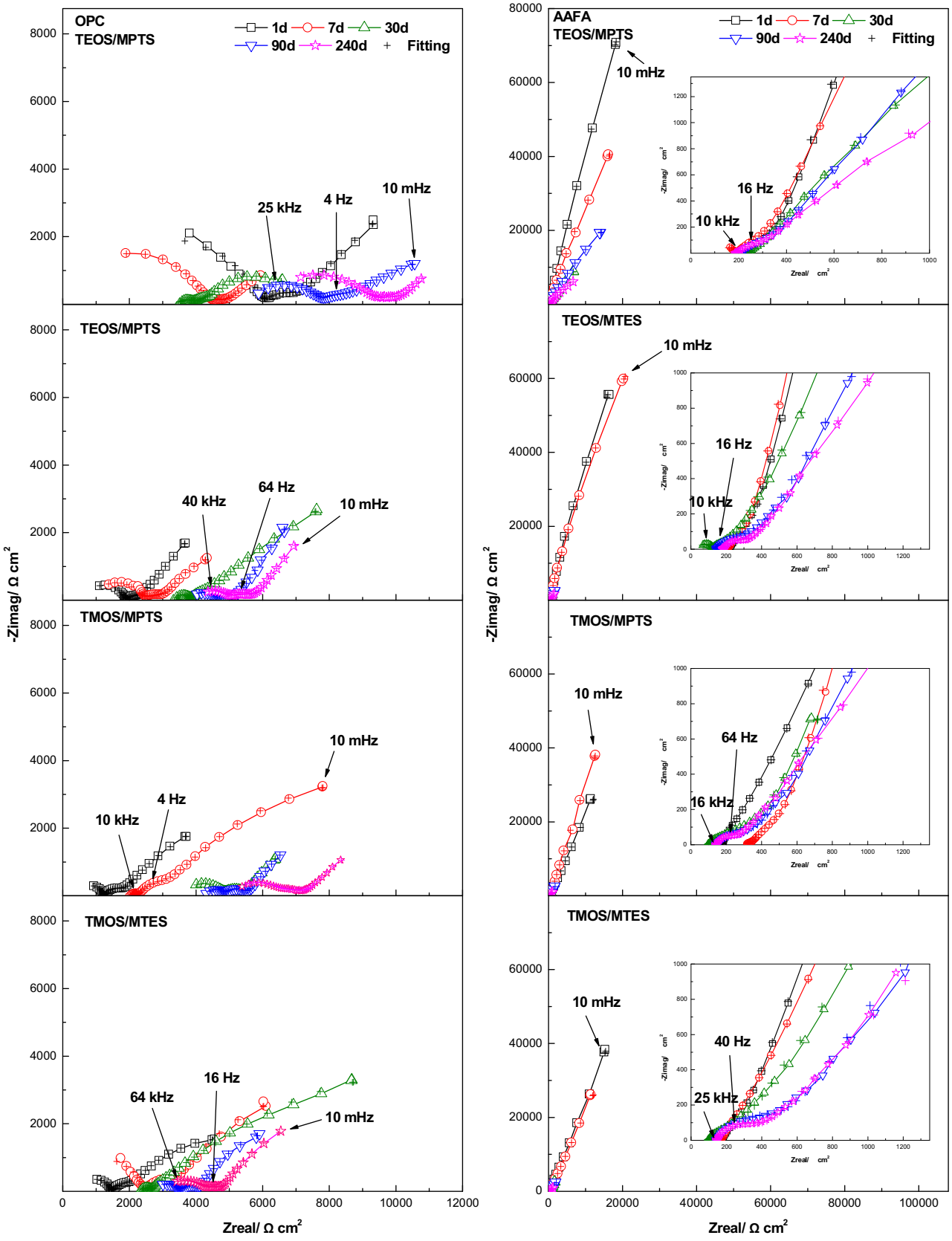

Fig. 5. Nyquist plots for coated rebars embedded in carbonated OPC and AAFA mortars over 240 days of immersion in a 3 wt.% NaCl solution.

intermediate frequency around 10^{-5}–10^{-4} F cm^{-2} $s^{-(1-\alpha_{IF})}$, and at low frequency in the order of mF cm^{-2} $s^{-(1-\alpha_{IF})}$, easily observable in the Nyquist plot (see Figs. 4 and 5). It should be noted that Bode plots (not included) did not allow visual observation of the three time constants described in the fitting process.

Table 3
Parameters used in the fitting of impedance data for the carbonated OPC mortar with uncoated steel rebar after different times of immersion in a 3 wt.% NaCl solution. The error, in%, associated with each parameter value is given in parenthesis.

Time Day	R_e Ω cm^2	Y_m, nF cm^{-2} $s^{-(1-\alpha_{HF})}$	α_m	R_m Ω cm^2	Y_f, μF cm^{-2} $s^{-(1-\alpha_{IF})}$	α_f	R_f Ω cm^2	Y_{dl}, mF cm^{-2} $s^{-(1-\alpha_{LF})}$	α_{dl}	R_{ct} KΩ cm^2
1	0	61 (9)	0.64 (1)	1251 (6)	480 (8)	0.50 (3)	662 (6)	5 (7)	0.65 (5)	3 (13)
7	0	64 (12)	0.62 (1)	2161 (1)	91 (13)	0.71 (4)	659 (6)	2 (5)	0.53 (5)	13 (15)
30	1910 (1)	1061 (13)	0.55 (3)	770 (4)	121 (10)	0.65 (3)	318 (5)	3 (1)	0.56 (2)	22 (13)
90	2617 (1)	602 (20)	0.76 (8)	416 (8)	142 (11)	0.62 (5)	1269 (7)	3 (13)	0.67 (7)	4 (17)
240	3350 (1)	370 (8)	0.58 (2)	1863 (2)	67 (6)	0.65 (2)	594 (3)	2 (1)	0.70 (3)	5 (8)

The dielectric properties of the bulk matrix, passive film or hybrid coating film and electrochemical behaviour at the steel/mortar interface can be quantified by fitting an appropriate electrical equivalent circuit (EEC) model to the EIS data. In the present study the EEC shown in Fig. 6 was utilized, obtained using *ZView* Software for the fitting process. The chi-square (χ^2) value was of the order of 10^{-3} in all cases, indicating a good fit. In the EEC a constant phase element (*CPE*) was used instead of a pure capacitor in order to consider the non-homogeneity of the studied system, which mainly comes from irregularities on the steel surface, surface roughness, fractal surface and in general certain processes associated with an irregular distribution of the applied potential [11,41]. The electrical impedance of a *CPE* is defined by the expression: $Z_{CPE} = \left(Y_p\right)^{-1}(j\omega)^{-\alpha}$, where Y_p is the admittance, ω is the angular frequency equal to $2\pi f$, f is the applied frequency, 2π is the habitual conversion constant, $j^2 = (-1)$ is the imaginary unit, and α, defined as the *CPE* power, is in the range $-1 < \alpha < 1$. When $\alpha = 0$, *CPE* is a resistor; when $\alpha = 1$, it is an ideal capacitor; and when $\alpha = -1$, it is an inductor. Finally, if $\alpha = 0.5$, the *CPE* is the Warburg admittance. R_e in Fig. 6 accounts for the electrolyte resistance, which is associated with the ionic mobility in a solution. R_m and Y_m are associated with

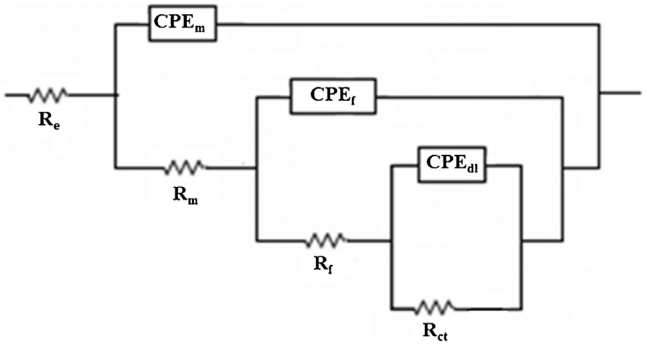

Fig. 6. Equivalent electrical circuit (EEC) for carbonated OPC and AAFA with uncoated and coated steel rebars.

Table 4
Parameters used in the fitting of impedance data for the carbonated AAFA mortar with uncoated steel rebar after different times of immersion in a 3 wt.% NaCl solution. The error, in%, associated with each parameter value is given in parenthesis.

Time Day	R_e Ω cm^2	Y_m, μF cm^{-2} $s^{-(1-\alpha_{HF})}$	α_m	R_m Ω cm^2	Y_f, μF cm^{-2} $s^{-(1-\alpha_{IF})}$	α_f	R_f Ω cm^2	Y_{dl} μF cm^{-2} $s^{-(1-\alpha_{LF})}$	α_{dl}	R_{ct} kΩ cm^2
1	347 (1)	10 (9)	0.78 (12)	56 (17)	59 (7)	0.86 (8)	550 (16)	63 (13)	0.85 (5)	3334 (17)
7	282 (1)	19 (13)	0.69 (18)	41 (14)	128 (12)	0.76 (13)	332 (13)	110 (17)	0.76 (9)	700 (12)
30	110 (2)	36 (13)	0.63 (11)	28 (18)	249 (12)	0.66 (7)	264 (17)	562 (11)	0.71 (3)	909 (15)
90	200 (2)	4 (9)	0.55 (12)	106 (4)	85 (19)	0.68 (4)	286 (7)	633 (2)	0.60 (1)	2630 (13)
240	250 (1)	1 (18)	0.57 (5)	163 (2)	148 (17)	0.60 (4)	211 (9)	513 (9)	0.66 (4)	2 (16)

Table 5
Parameters used in the fitting of impedance data for the carbonated OPC mortar with coated steel rebar after different times of immersion in a 3 wt.% NaCl solution. The error, in%, associated with each parameter value is given in parenthesis.

Time Day	R_e Ω cm^2	Y_m, nF cm^{-2} $s^{-(1-\alpha_{HF})}$	α_m	R_m Ω cm^2	Y_f, μF cm^{-2} $s^{-(1-\alpha_{IF})}$	α_f	R_f Ω cm^2	Y_{dl}, mF cm^{-2} $s^{-(1-\alpha_{LF})}$	α_{dl}	R_{ct} KΩ cm^2
TEOS/MPTS										
1	0	10 (10)	0.72 (1)	6030 (6)	80 (12)	0.62 (11)	1124 (18)	1 (12)	0.55 (12)	34 (16)
7	0	10 (3)	0.78 (1)	4130 (1)	250 (17)	0.49 (6)	1099 (9)	3 (6)	0.58 (7)	7 (18)
30	3472 (1)	2965 (18)	0.63 (6)	475 (4)	413 (18)	0.45 (7)	1288 (17)	5 (18)	0.92 (17)	2 (12)
90	5469 (1)	413 (13)	0.61 (2)	2331 (8)	87 (19)	0.64 (19)	720 (18)	1 (18)	0.41 (19)	10 (17)
240	5543 (1)	291 (8)	0.54 (1)	3901 (2)	218 (18)	0.49 (13)	934 (16)	2 (6)	0.61 (3)	9 (18)
TEOS/MTES										
1	628 (2)	49 (6)	0.77 (1)	1276 (1)	267 (10)	0.58 (4)	507 (6)	2 (1)	0.58 (2)	50 (18)
7	873 (12)	64 (15)	0.79 (8)	1330 (14)	514 (17)	0.38 (14)	2018 (6)	2 (18)	0.83 (10)	25 (10)
30	3404 (1)	89 (19)	0.92 (9)	357 (14)	403 (17)	0.43 (10)	2151 (16)	0.4 (11)	0.59 (10)	23 (16)
90	3855 (1)	306 (14)	0.69 (2)	764 (8)	133 (8)	0.48 (4)	718 (4)	2 (13)	0.68 (7)	30 (17)
240	4043 (1)	160 (15)	0.71 (2)	801 (2)	211 (3)	0.41 (2)	1390 (3)	2 (1)	0.72 (3)	30 (19)
TMOS/MPTS										
1	228 (14)	58 (6)	0.71 (1)	1039 (3)	98 (4)	0.75 (1)	580 (2)	2 (1)	0.60 (1)	10 (3)
7	2066 (1)	535 (11)	0.84 (9)	208 (12)	92 (16)	0.67 (5)	1183 (10)	0.6 (2)	0.61 (2)	12 (5)
30	3729(1)	49 (11)	0.81 (4)	909 (6)	221 (8)	0.48 (2)	1137 (5)	4 (5)	0.68 (4)	11 (18)
90	4323 (1)	205 (9)	0.79 (8)	550 (3)	40 (12)	0.64 (6)	702 (6)	2 (3)	0.62 (4)	14 (14)
240	4972 (1)	834 (10)	0.56 (2)	1608 (4)	193 (11)	0.48 (17)	917 (16)	3 (5)	0.60 (3)	9 (18)
TMOS/MTES										
1	421 (6)	47 (8)	0.75 (1)	1067 (2)	153 (6)	0.67 (2)	725 (4)	1 (1)	0.63 (1)	5 (2)
7	0	5 (17)	0.85 (2)	2419 (1)	190 (11)	0.55 (7)	1465 (14)	1 (9)	0.76 (7)	8 (13)
30	2366 (1)	396 (14)	0.82 (8)	280 (8)	214 (1)	0.57 (1)	2075 (5)	0.3 (1)	0.49 (3)	15 (6)
90	2778 (1)	416 (13)	0.66 (7)	774 (7)	107 (13)	0.62 (5)	638 (6)	2 (2)	0.71 (2)	6 (4)
240	2922 (1)	1295 (15)	0.52 (5)	1442 (6)	207 (19)	0.51 (11)	553 (15)	2 (3)	0.70 (2)	8 (5)

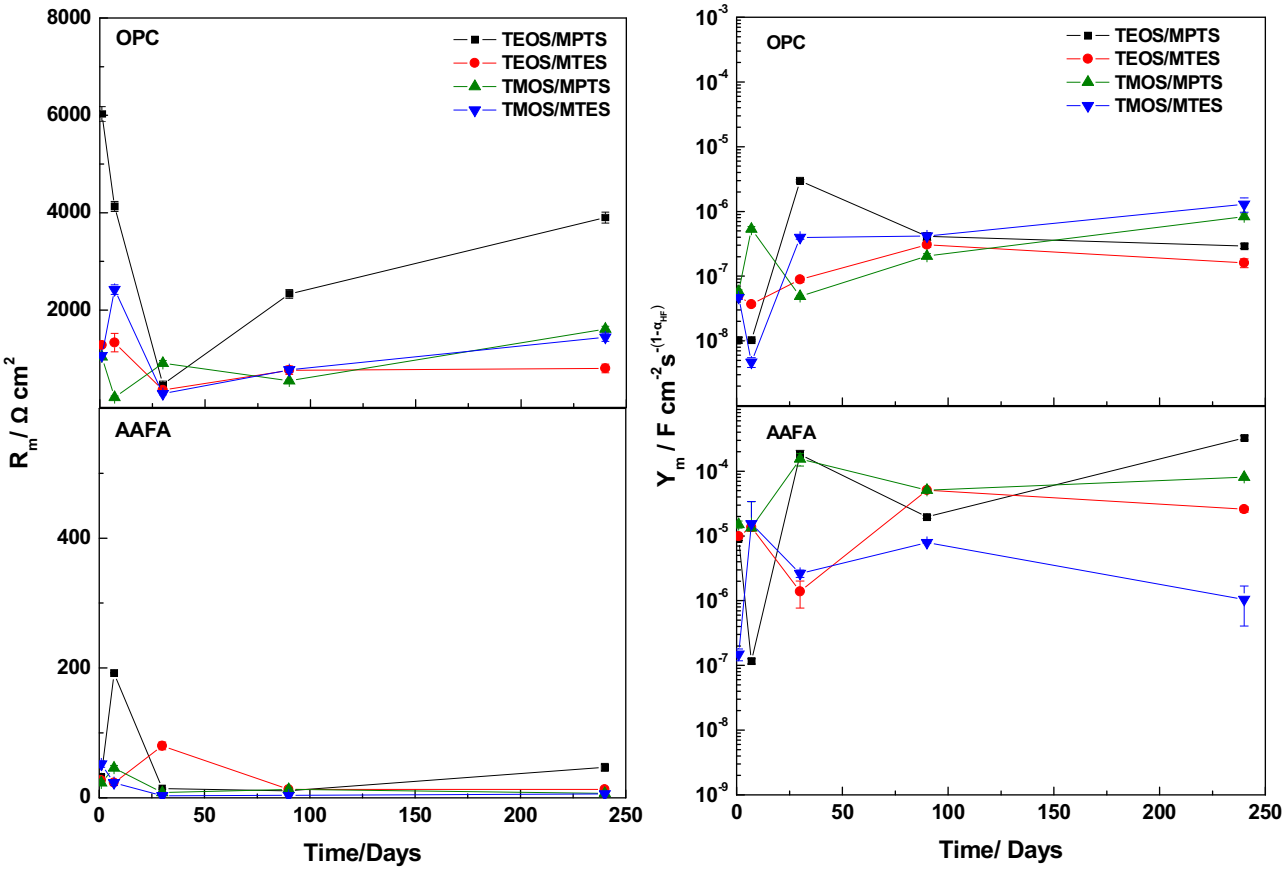

Fig. 7. Bulk-matrix resistance (R_m) and capacitance (Y_m) values of coated steel rebars synthesized with TEOS/MPTS, TEOS/MTES, TMOS/MPTS or TMOS/MTES mixtures and embedded in carbonated OPC and AAFA mortars for 240 days of immersion in a 3 wt.% NaCl solution. Left: R_m. Right: Y_m.

the bulk matrix resistance and capacitance, respectively. The bulk matrix resistance reflects the ability of the mortar to hinder the penetration of electrolytes containing aggressive ions and the bulk matrix capacitance reflects the dielectric properties of the mortars. R_f and Y_f indicate the passive film or hybrid coating film resistance and capacitance, respectively. Finally, as indicated above, R_{ct} and

Table 6
Parameters used in the fitting of impedance data for the carbonated AAFA mortar with coated steel rebar after different times of immersion in a 3 wt.% NaCl solution. The error, in%, associated with each parameter value is given in parenthesis.

Time Day	R_e Ω cm^2	Y_m, μF cm^{-2} $s^{-(1-\alpha_{HF})}$	α_m	R_m Ω cm^2	Y_f, μF cm^{-2} $s^{-(1-\alpha_{IF})}$	α_f	R_f Ω cm^2	Y_{dl} μF cm^{-2} $s^{-(1-\alpha_{LF})}$	α_{dl}	R_{ct} kΩ cm^2
TEOS/MPTS										
1	201 (1)	9 (15)	0.73 (7)	33 (8)	61 (17)	0.86 (4)	316 (16)	80 (15)	0.89 (2)	1853 (14)
7	0	0.1 (12)	0.74 (2)	192 (1)	132 (4)	0.76 (1)	396 (7)	80 (6)	0.91 (1)	517 (11)
30	228 (1)	180 (16)	0.53 (2)	14 (10)	240 (16)	0.73 (5)	274 (16)	144 (16)	0.83 (5)	115 (15)
90	197 (1)	20 (14)	0.73 (2)	11 (15)	154 (7)	0.63 (1)	458 (6)	93 (6)	0.83 (1)	161 (6)
240	182 (1)	328 (7)	0.50 (3)	48 (16)	6 (16)	0.99 (8)	284 (11)	165 (12)	0.77 (2)	62 (11)
TEOS/MTES										
1	201 (1)	9 (13)	0.80 (15)	27 (19)	72 (12)	0.85 (5)	369 (17)	101 (15)	0.87 (2)	1113 (16)
7	200 (1)	14 (14)	0.78 (16)	23 (15)	69 (12)	0.84 (6)	326 (16)	80 (15)	0.89 (2)	648 (9)
30	46 (9)	1 (14)	0.75 (6)	80 (7)	1010 (14)	0.62 (8)	187 (19)	3086 (10)	0.73 (4)	9491 (16)
90	135 (13)	51 (14)	0.57 (15)	13 (8)	294 (5)	0.57 (7)	298 (15)	1864 (5)	0.69 (7)	9472 (11)
240	174 (1)	26 (15)	0.67 (3)	13 (14)	134 (16)	0.60 (4)	178 (5)	1834 (1)	0.62 (3)	270 (15)
TMOS/MPTS										
1	153 (1)	15 (13)	0.70 (17)	23 (19)	159 (12)	0.74 (4)	894 (17)	89 (18)	0.72 (4)	12241 (18)
7	319 (1)	13 (15)	0.75 (19)	46 (13)	74 (13)	0.81 (9)	326 (11)	154 (16)	0.83 (3)	1464 (16)
30	90 (12)	154 (11)	0.59 (19)	8 (6)	1537 (18)	0.56 (17)	516 (15)	6311 (12)	0.80 (11)	344 (17)
90	135 (13)	51 (9)	0.57 (18)	13 (17)	294 (16)	0.57 (15)	298 (15)	1864 (6)	0.69 (4)	9472 (10)
240	139 (1)	1 (14)	1.00 (16)	7 (18)	105 (11)	0.70 (2)	146 (3)	1640 (5)	0.59 (3)	1816 (12)
TMOS/MTES										
1	120 (4)	0.1 (18)	0.86 (12)	52 (9)	127 (1)	0.73 (1)	449 (3)	75 (2)	0.82 (1)	16021 (12)
7	153 (1)	15 (12)	0.70 (17)	23 (19)	159 (16)	0.74 (4)	895 (16)	88 (18)	0.72 (4)	19889 (16)
30	97 (2)	3 (13)	1.00 (8)	3 (10)	591 (12)	0.58 (7)	350 (12)	1401 (11)	0.66 (5)	20864 (13)
90	139 (1)	7 (13)	0.80 (12)	4 (13)	175 (15)	0.61 (4)	447 (7)	1749 (2)	0.61 (3)	15397 (16)
240	141 (1)	1 (11)	1.00 (5)	6 (17)	96 (12)	0.68 (3)	270 (5)	2096 (1)	0.53 (3)	2576 (15)

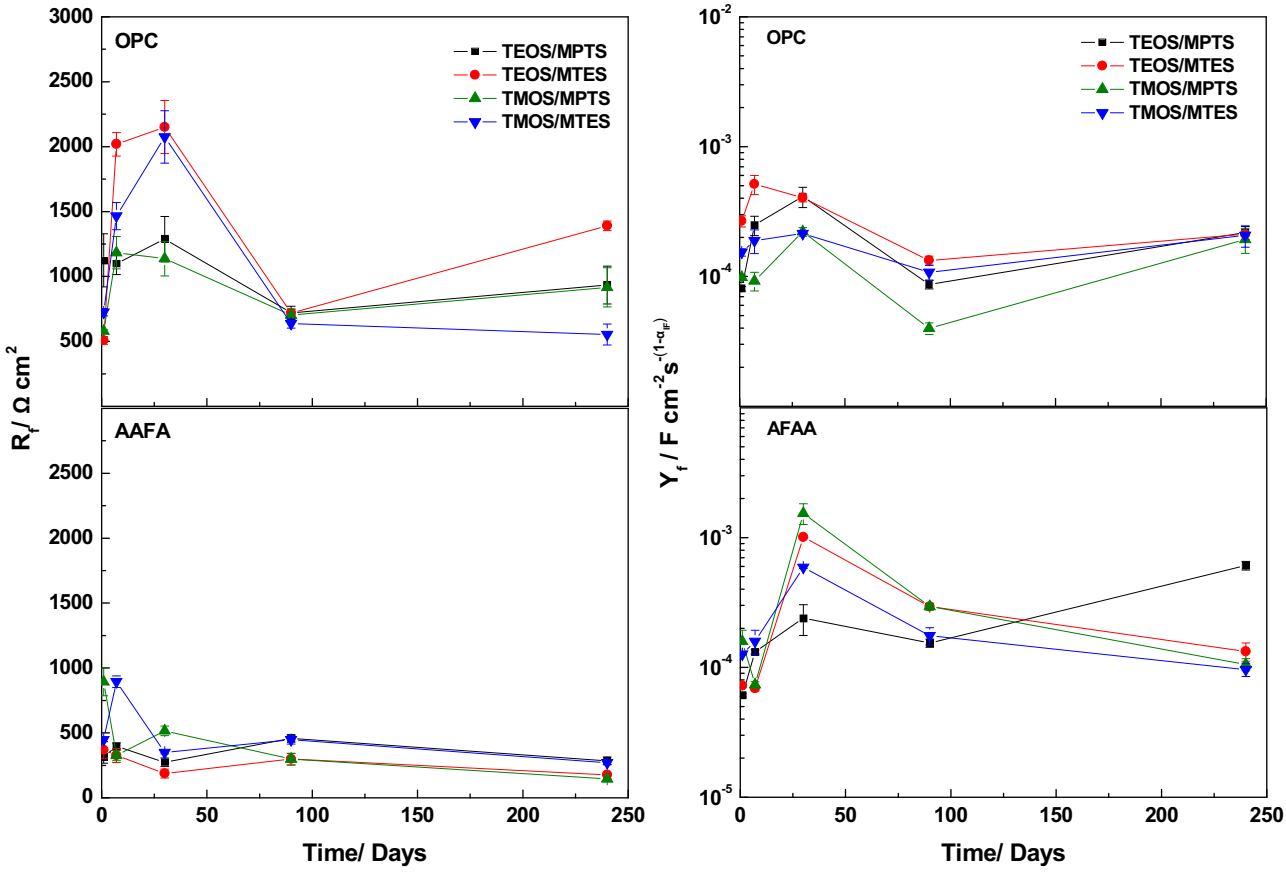

Fig. 8. Coating resistance (R_f) and capacitance (Y_f) values of coated steel rebars synthesized with TEOS/MPTS, TEOS/MTES, TMOS/MPTS or TMOS/MTES mixtures and embedded in carbonated OPC and AAFA mortars for 240 days of immersion in a 3 wt.% NaCl solution. Left: R_f. Right: Y_f.

Y_{dl} are associated with the charge transfer resistance of the corrosion process and the double-layer capacitance, respectively. A model similar to this was used to study the electrochemical characteristics of enamel-coated steel rebars embedded in OPC mortar [41].

Tables 3 and 4 list the EEC parameter values obtained by fitting the Nyquist plots recorded for carbonated OPC and AAFA mortars, respectively, with the uncoated steel rebar after different immersion times (up to 240 days) in the NaCl-rich solution. R_e values show a tendency to increase over exposure time in OPC mortar, probably due to the mortar curing process, which induces a long-term decrease in the mortar porosity and an increase in its resistivity. R_e values are in the range of 110–347 Ω cm^2 for the AAFA mortar (see Table 4). The decrease in the R_e parameter may be attributed to a high concentration of dissolved salts in the mortar pore network solution.

The R_m parameter is in the range of 416–1863 Ω cm^2 for uncoated steel embedded in carbonated OPC mortar, and in the range of 28–163 Ω cm^2 for uncoated steel embedded in carbonated AAFA mortar. The Y_m parameter is in the range of 61–1061 nF cm^{-2} $s^{-(1-\alpha_{HF})}$ for OPC mortar and 1–36 μF cm^{-2} $s^{-(1-\alpha_{HF})}$ for AAFA mortar. These lower R_m values and higher Y_m values for AAFA mortar may be due the formation of different reaction products in the cementitious systems, and the presence of a more electrically conductive solution inside the carbonated AAFA mortar than in OPC mortar. In AAFA mortar the penetration of CO_2 favours the formation of sodium carbonate while in OPC mortar it produces the more insoluble calcium carbonate [10,52].

At intermediate frequency the R_f parameter is in the range of 318–1269 Ω cm^2 and the Y_f parameter is in the range of 67–480 μF cm^{-2} $s^{-(1-\alpha_{IF})}$ for uncoated steel embedded in carbonated OPC mortar. For uncoated steel rebars embedded in carbonated AAFA mortar the R_f and Y_f values are of the same order of magnitude. Finally, at low frequencies the R_{ct} parameter is as high as 3.3×10^6 Ω cm^2 for the uncoated steel embedded in AAFA mortar, and this parameter always is higher than for uncoated steel embedded in OPC mortar. This indicates a higher corrosion resistance of the steel reinforcement in these new mortar types (AAFA). R_{ct} presents a continuous decrease with immersion time (~2–5 kΩ cm^2), indicating a transition from the passive state to the active state. With time, an increase in the chloride ion concentration takes place on the metal surface and more corrosion pits are formed on the passive film, leading to its eventual breakdown. The Y_{dl} parameter is in the range of 2–5 mF cm^{-2} $s^{-(1-\alpha_{LF})}$ for OPC mortar and in the range of 63–633 μF cm^{-2} $s^{-(1-\alpha_{LF})}$ for AAFA mortar. The Y_{dl} values increases with exposure time for AAFA mortar, but these values are always lower than for OPC mortar. The lower Y_{dl} values of AAFA mortar also indicates higher corrosion resistance.

Accepting that the Stern-Geary equation can be applied, with an approximate B constant value of 52 or 26 mV, the resulting i_{corr} is 1.04 μA cm^{-2} for OPC mortar and 0.06 μA cm^{-2} for AAFA mortar after 30 days, showing steels in the active and passive state, respectively. These results are not far from the i_{corr} results obtained using LPR measurements (see Fig. 3).

Tables 5 and 6 list EEC parameter values obtained by fitting the Nyquist plots recorded for carbonated OPC and AAFA mortars with the different coated steel rebars after different immersion times (up to 240 days) in the NaCl-rich solution. The R_e values for coated steels embedded in OPC mortar are in the range of 228–5469 Ω cm^2, and are lower, between 46–319 Ω cm^2 in the case of the coated steels

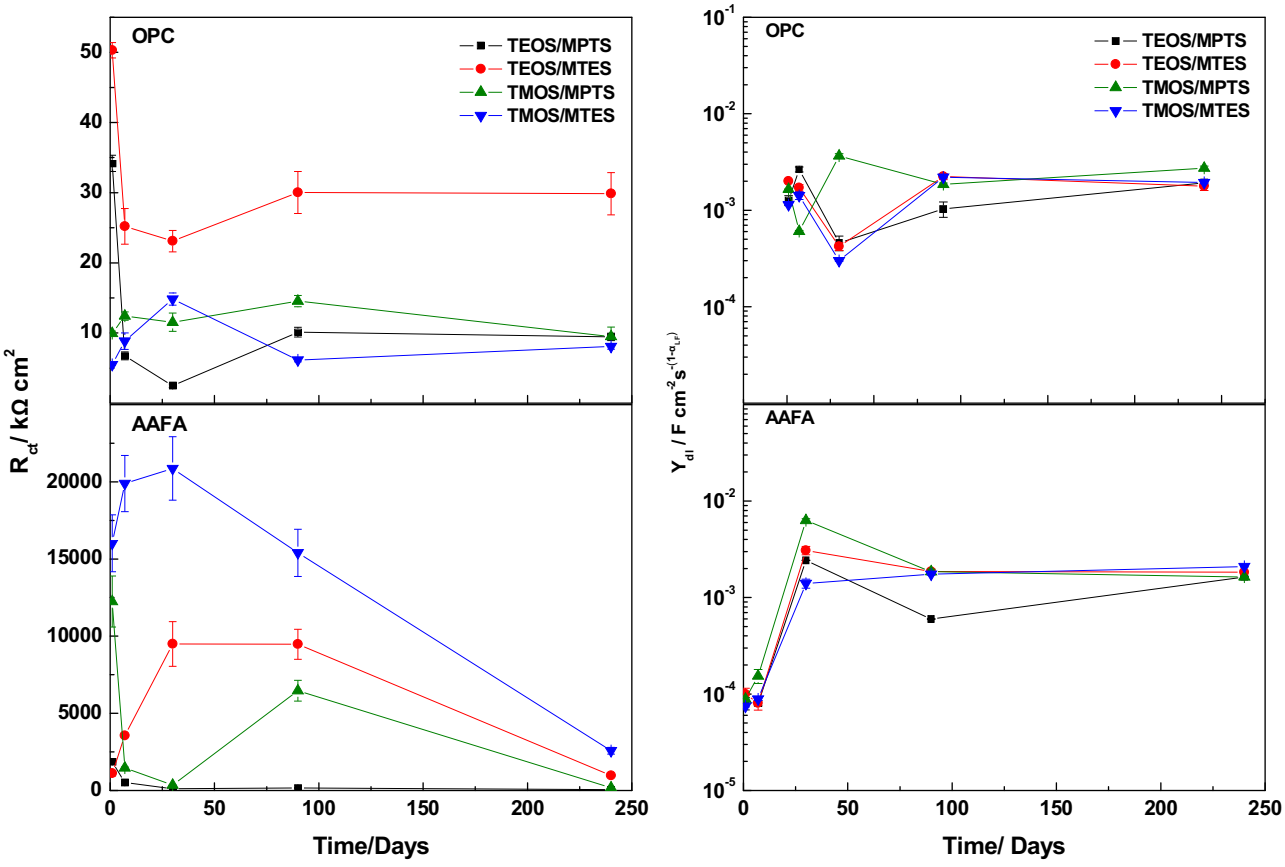

Fig. 9. Charge transfer resistance (R_{ct}) and double-layer capacitance (Y_{dl}) values for coated steel rebars synthesized with TEOS/MPTS, TEOS/MTES, TMOS/MPTS or TMOS/MTES mixtures and embedded in carbonated OPC and AAFA mortars for 240 days of immersion in a 3 wt.% NaCl solution. Left: R_{ct}. Right: Y_{dl}.

embedded in AAFA mortar. This decrease in the R_e parameter may be associated with a high level of sodium salts from the activating solutions which are found in the pores of the latter mortar when carbonated [10,11].

Fig. 7 displays the changes in the bulk-matrix resistance (R_m) and capacitance (Y_m) parameters over time for coated steel rebars synthesized with the TEOS/MPTS, TEOS/MTES, TMOS/MPTS or TMOS/MTES mixtures and embedded in carbonated OPC and AAFA mortars immersed in the NaCl-rich solution. R_m values are in the 208–6030 Ω cm^2 range for OPC mortar and in the 3–192 Ω cm^2 range for AAFA mortar, approximately thirty times lower. OPC mortar presents higher resistivity than AAFA mortar, and the open pore structure of OPC mortar is lower due to fact that the calcium carbonate formed in these system is more insoluble than sodium carbonate formed in the AAFA system. Y_m values are in the ranges of 5–2970 nF cm^{-2} $s^{-(1-\alpha_{HF})}$ and 0.1 – 328 μF cm^{-2} $s^{-(1-\alpha_{HF})}$ for OPC and AAFA mortars, respectively. In most of the mortars assessed these ranges are of the same order as those obtained for the uncoated steel embedded in OPC and AAFA mortars. Moreover, the range of Y_m value OPC mortar is in reasonable agreement with what has been reported in the literature [51,53].

Fig. 8 shows the changes in the R_f and Y_f parameters with time for coated steel with TEOS/MPTS, TEOS/MTES, TMOS/MPTS or TMOS/MTES mixtures embedded in carbonated OPC and AAFA mortars after different exposure times to 3 wt.% NaCl solution. The R_f and Y_f parameters measure the barrier performance of the hybrid coatings against the penetration of water and chloride ions [54,55]. Irrespective of the coating deposited on the steel surface, R_f values are higher for OPC mortar than for AAFA mortar. This may be attributed to a slightly lower deterioration of the coating in this system, and a slower access of aggressive species to the steel. The Y_f parameter varies in the range of 40 – 514 μF cm^{-2} $s^{-(1-\alpha_{IF})}$ for carbonated OPC mortar and 61–540 μF cm^{-2} $s^{-(1-\alpha_{IF})}$ for carbonated AAFA mortar. The higher values for the AAFA mortar indicate that the coatings deposited on the steel present a slightly higher number of open channels allowing easier water uptake.

Fig. 9 displays the changes in the R_{ct} and Y_{dl} parameters of the coated steel with TEOS/MPTS, TEOS/MTES, TMOS/MPTS or TMOS/MTES mixtures and embedded in carbonated OPC and AAFA mortars after different immersion times in 3 wt.% NaCl solution. These parameters are associated with the corrosion process. For carbonated OPC mortar, R_{ct} values remain fairly constant over the immersion time, within the range of $2.5 \times 10^3 - 50.3 \times 10^3$ kΩ cm^2. However, for carbonated AAFA mortar this parameter experiences a continuous reduction over the exposure time to chlorides, presenting values within the range of $20.9 \times 10^6 - 61.7 \times 10^3$ Ω cm^2. After 240 days of exposure the R_{ct} values indicate that steel embedded in OPC mortar is in an active state, while the steels embedded in AAFA mortar remain in a passive state for a longer time period. The Y_{dl} parameter is in the range of 0.3–3.7 mF cm^{-2} $s^{-(1-\alpha_{LH})}$ for coated steel embedded in carbonated OPC mortar and 75–6300 μF cm^{-2} $s^{-(1-\alpha_{LF})}$ for AAFA mortar. The lower Y_{dl} values indicate a higher corrosion resistance for this new type of mortar (AAFA), although these values at the end of the test are similar to those obtained for OPC mortar. This behaviour may indicate an increase in corrosion activity at the double-layer interface by the diffusion of chloride ions. In the light of the EIS results, carbonated AAFA mortar in the presence of chloride ions shows higher corrosion resistance than OPC mortar probably due to the higher concentration of silicate anions in the pore solution of the AAFA mortar which is capable of delaying the corrosion process [49,50]. A dense and compact structure, higher dimensionality and degree of condensation [34],

greater adherence to the steel, and higher atomic percentage of Si in its composition [33] lead to a low electrolyte diffusion rate through the film and protect the steel rebar against corrosion. These results are in agreement with those obtained using direct current (DC) measurements, shown in Fig. 3.

4. Conclusions

Corrosion of coated steel rebars embedded in carbonated OPC and AAFA mortars in the presence of chloride ions is not only dependent on the type of the cementitious system but also on the nature of the reagents forming the coating. AAFA mortar is more efficient against rebar corrosion than OPC mortar (high E_{corr} values and low i_{corr} values), as the silicate present in the alkaline solution used to activate the FA may act as a steel corrosion inhibitor. The organic-inorganic hybrids synthesized with TEOS/MTES and TMOS/MTES for carbon steel embedded in carbonated AAFA mortar present the lowest i_{corr} values, indicating that these coatings afford the best protective properties over 240 days of exposure.

Acknowledgements

M. Criado expresses her gratitude to the Spanish Ministry of Science and Innovation for the Juan de la Cierva contract (Ref. JDC-2010). Comments from Dr. S.A. Bernal (U. Sheffield) are greatly acknowledged.

References

[1] E. Gartner, Industrially interesting approaches to low-CO_2 cements, Cem. Concr. Res. 34 (2004) 1489–1498.
[2] A. Palomo, P. Krivenko, I. Garcia-Lodeiro, E. Kavalerova, O. Maltseva, A. Fernández-Jiménez, A review on alkaline activation: new analytical perspectives, Mater. Constr. 64 (2014) e022.
[3] P. Duxson, J.L. Provis, Designing precursors for geopolymer cements, J. Am. Ceram. Soc. 91 (2008) 3864–3869.
[4] J. Davidovits, Geopolymers: inorganic polymeric new materials, J. Therm. Anal. 37 (1991) 1633–1656.
[5] P. Duxson, A. Fernández-Jiménez, J.L. Provis, G.C. Lukey, A. Palomo, J.S.J. Van Deventer, Geopolymer technology: the current state of the art, J. Mater. Sci. 42 (2007) 2917–2933.
[6] A. Palomo, M.W. Grutzeck, M.T. Blanco, Alkali-activated fly ashes: a cement for the future, Cem. Concr. Res. 29 (1999) 1323–1329.
[7] D. Hardjito, S.E. Wallah, D.M.J. Sumajouw, B.V. Rangan, On the development of fly ash-based geopolymer concrete, ACI Mater. J. 101 (2004) 467–472.
[8] F. Winnefeld, A. Leemann, M. Lucuk, P. Svoboda, M. Neuroth, Assessment of phase formation in alkali activated low and high calcium fly ashes in building materials, Constr. Build. Mater. 24 (2010) 1086–1093.
[9] A. Fernández-Jiménez, A. Palomo, Composition and microstructure of alkali activated fly ash binder: effect of the activator, Cem. Concr. Res. 35 (2005) 1984–1992.
[10] M. Criado, C. Monticelli, S. Fajardo, D. Gelli, V. Grassi, J.M. Bastidas, Organic corrosion inhibitor mixtures for reinforcing steel embedded in carbonated alkali-activated fly ash mortar, Constr. Build. Mater. 35 (2012) 30–37.
[11] C. Monticelli, M. Criado, S. Fajardo, J.M. Bastidas, M. Abbottoni, A. Balbo, Corrosion behaviour of a low Ni austenitic stainless steel in carbonated chloride-polluted alkali-activated fly ash mortar, Cem. Concr. Res. 55 (2014) 49–58.
[12] M. Sufian-Badar, K. Kupwade-Patil, S.A. Bernal, J.L. Provis, E.N. Allouche, Corrosion of steel bars induced by accelerated carbonation in low and high calcium fly ash geopolymer concretes, Constr. Build. Mater. 61 (2014) 79–89.
[13] L. Bertolini, B. Elsener, P. Pedeferri, R. Polder, Corrosion of Steel in Concrete-Prevention, Diagnosis, Repair, Wiley-VCH, Weinheim, 2004.
[14] J.A. Gónzalez, Prediction of reinforced concrete structure durability by electrochemical techniques, Corrosion 63 (2007) 811–818.
[15] U. Angst, B. Elsener, C.K. Larsen, Ø. Vennesland, Critical chloride content in reinforced concrete-a review, Cem. Concr. Res. 39 (2009) 1122–1138.
[16] N.M. Ihekwaba, B.B. Hope, C.M. Hansson, Carbonation and electrochemical chloride extraction from concrete, Cem. Concr. Res. 26 (1996) 1095–1107.
[17] S. Pour-Ali, C. Dehghanian, A. Kosari, Corrosion protection of the reinforcing steels in chloride-laden concrete environment through epoxy/polyaniline-camphorsulfonate nanocomposite coating, Corros. Sci. 90 (2015) 239–247.
[18] M. Książek, The evaluate tendencies of corrosion process for reinforcing steel when covered with special polymer sulfur coating, Eng. Fail. Anal. 39 (2014) 1–11.
[19] M. Barletta, M. Puopolo, A. Gisario, S. Vesco, Application and drying at ambient temperature of thick organic-inorganic hybrid coatings on glass, Surf. Coat. Techol. 236 (2013) 212–223.
[20] J.X. Bi, C.H. Yang, H.T. Wu, Synthesis characterization, and microwave dielectric properties of Ni0.5Ti0.5NbO4 ceramics through the aqueous sol-gel process, J. Alloy. Compd. 653 (2015) 1–6.
[21] J. Graffion, A.M. Cojocariu, X. Cattoën, R.A.S. Ferreira, V.R. Fernandes, P.S. André, L.D. Carlos, M. Wong Chi Man, J.R. Bartlett, Luminescent coatings from bipyridine-based bridged silsesquioxanes containing Eu^{3+} and Tb^{3+} salts, J. Mater. Chem. 22 (2012) 13279–13285.
[22] E. Kiele, J. Senvaitiene, A. Griguceviciene, R. Ramanauskas, R. Raudonis, A. Kareiva, Application of sol-gel method for the conservation of copper alloys, Microchem. J. 124 (2016) 623–628.
[23] Z.N. Kayani, A. Munir, S. Riaz, S. Naseem, Structural, optical and magnetic properties of aluminum doped MnZnO films deposited by dip coating, J. Alloy. Compd. 662 (2016) 489–496.
[24] L. Ćurković, H.O. Ćurković, S. Salopek, M.M. Renjo, S. Šegota, Enhancement of corrosion protection of AISI 304 stainless steel by nanostructured sol-gel TiO_2 films, Corros. Sci. 77 (2013) 176–184.
[25] T.T. Phan, F. Bentiss, C. Jama, Structural and anticorrosion performance characterization of phosphosilicate sol-gel coatings prepared from 3-(trimethoxysilyl) propyl methacrylate and bis[2-(methacryloyloxy)ethyl] phosphate, Prog. Org. Coat. 89 (2015) 123–131.
[26] P. Judeinstein, C.J. Sanchez, Hybrid organic-inorganic materials: a land of multidisciplinarity, J. Mater. Chem. 6 (1996) 511–525.
[27] I. Zaręba-Grodź, W. Mišta, W. Stręk, E. Bukowska, K. Hermanowicz, K. Maruszewski, Synthesis and properties of an inorganic-organic hybrid prepared by the sol-gel method, Opt. Mater. 26 (2004) 207–211.
[28] M. Houmard, D.C.L. Vasconcelos, W.L. Vasconcelos, G. Berthomé, J.C. Joud, M. Langlet, Water and oil wettability of hybrid organic-inorganic titanate-silicate thin films deposited via a sol-gel route, Surf. Sci. 603 (2009) 2698–2707.
[29] C.J. Brinker, G.W. Scherer, Sol-gel Science The Physics and Chemistry of Sol-gel Processing, Academic Press, San Diego, 1990.
[30] T. Minami, N. Tohge, Formation of inorganic coatings on polymer films by the sol-gel method, New Glass 9 (1994) 23–28.
[31] V. Barranco, N. Carmona, J.C. Galván, M. Grobelny, L. Kwiatkowski, M.A. Villegas, Electrochemical study of tailored sol-gel thin films as pre-treatment prior to organic coating for AZ91 magnesium alloy, Prog. Org. Coat. 68 (2010) 347–355.
[32] M. Criado, I. Sobrados, J. Sanz, J.M. Bastidas, Steel protection using sol-gel coatings in simulated concrete pore solution contaminated with chlorides, Surf. Coat. Technol. 258 (2014) 485–494.
[33] M. Criado, I. Sobrados, J.M. Bastidas, J. Sanz, Steel corrosion in simulated carbonated concrete pore solution its protection using sol-gel coatings, Prog. Org. Coat. 88 (2015) 228–236.
[34] M. Criado, I. Sobrados, J. Sanz, Polymerization of hybrid organic-inorganic materials from several silicon compounds followed by TGA/DTA, FTIR and NMR techniques, Prog. Org. Coat. 77 (2014) 880–891.
[35] M. Criado, I. García-Díaz, J.M. Bastidas, F.J. Alguacil, F.A. López, C. Monticelli, Effect of recycled glass fiber on the corrosion behavior of reinforced mortar, Constr. Build. Mater. 64 (2014) 261–269.
[36] ASTM E104-02 Standard, Maintaining Constant Relative Humidity by Means of Aqueous Solutions, (2012).
[37] M. Stern, A.L. Geary, Electrochemical polarization I. A theoretical analysis of the shape of polarization curves, J. Electrochem. Soc. 104 (1957) 56–63.
[38] C. Andrade, V. Castelo, C. Alonso, J.A. González, The determination of the corrosion rate of steel embedded in concrete by the polarization resistance and AC impedance methods, in: STP 906, Corrosion of Rebar in Concrete, ASTM, Philadelphia, PA, 1984.
[39] ASTM C876-09 Standard, Test Method for Half-Cell Potentials of Uncoated Reinforcing Steel in Concrete, (2009).
[40] B. Elsener, C. Andrade, J. Gulikers, R. Polder, M. Raupach, RILEM TC 154-EMC recommendations: half-cell potential measurements-potential mapping on reinforced concrete structures, Mater. Struct. 36 (2003) 461–471.
[41] F. Tang, G. Chen, J.S. Volz, R.K. Brow, M.L. Koenigstein, Cement-modified enamel coating for enhanced corrosion resistance of steel reinforcing bars, Cem. Concr. Comp. 35 (2013) 171–180.
[42] T. Zafeiropoulou, E. Rakanta, G. Batis, Performance evaluation of organic coatings against corrosion in reinforced cement mortars, Prog. Org. Coat. 72 (2011) 175–180.
[43] Durar network specification manual inspection evaluation and assessment of Corrosion in reinforced concrete structures, CYTED Program, Rio de Janeiro, 1997.
[44] G. Fajardo, P. Valdez, J. Pacheco, Corrosion of steel rebar embedded in natural pozzolan based mortars exposed to chlorides, Construc. Build. Mater. 23 (2009) 768–774.
[45] P. Garcés, L.G. Andión, E. Zornoza, M. Bonilla, J. Payá, The effect of processed fly ashes on the durability and the corrosion of steel rebars embedded in cement–modified fly ash mortars, Cem. Concr. Compos. 32 (2010) 204–210.
[46] H.F.W. Taylor, Cement Chemistry, Academic Press, London, 1990.
[47] A. Palomo, S. Alonso, A. Fernández-Jiménez, I. Sobrados, J. Sanz, Alkaline activation of fly ashes. A ^{29}Si NMR study of the reactions products, J. Am. Ceram. Soc. 87 (2004) 1141–1145.
[48] A. Fernández-Jimenez, J.M. Miranda, J.A. González, A. Palomo, Steel passive state stability in activated fly ash mortars, Mater. Constr. 60 (2010) 51–65.

[49] S.T. Amaral, I.I. Müller, Passivation of pure iron in alkaline solution containing silicate and sulphate-galvanostatic and potentiostatic studies, Corros. Sci. 41 (1999) 747–758.
[50] S.T. Amaral, I.I. Müller, A RRDE study of the electrochemical behavior of iron in solutions containing silicate and sulphate at pH 10–13, Corros. Sci. 41 (1999) 759–771.
[51] K.K. Sagoe-Crentsil, F.P. Glasser, J.T.S. Irvine, Electrochemical characteristics of reinforced concrete corrosion as determined by impedance spectroscopy, Br. Corros. J. 27 (1992) 113–118.
[52] S.A. Bernal, J.L. Provis, B. Walkley, R. San Nicolas, J.D. Gehman, D.G. Brice, A.R. Kilcullen, P. Duxson, J.S.J. van Deventer, Gel nanostructure in alkali-activated binders based on slag and fly ash: and effects of accelerated carbonation, Cem. Concr. Res. 53 (2013) 127–144.
[53] W. Aperador, R. Mejía de Gutiérrez, D.M. Bastidas, Steel corrosion behaviour in carbonated alkali-activated slag concrete, Corros. Sci. 51 (2009) 2027–2033.
[54] F. Tang, G. Chen, R.K. Brow, J.S. Volz, M.L. Koenigstein, Corrosion resistance and mechanism of steel rebar coated with three types of enamel, Corros. Sci. 59 (2012) 157–168.
[55] F. Tang, X. Chen, G. Chen, R.K. Brow, J.S. Volz, M.L. Koenigstein, Electrochemical behavior of enamel-coated carbon steel in simulated concrete pore water solution with various chloride concentrations, Electrochim. Acta 92 (2013) 36–46.